Available online at www.sciencedirect.com
SCIENCE DIRECT®
Journal of Sound and Vibration 276 (2004) 933–956
JOURNAL OF SOUND AND VIBRATION
www.elsevier.com/locate/jsvi

An equivalent model for smart beams with debonded piezoelectric patches

Dongchang Sun, Liyong Tong*

School of Aerospace, Mechanical and Mechatronic Engineering, The University of Sydney, Sydney, NSW 2006, Australia

Received 16 August 2002; accepted 6 August 2003

Abstract

An equivalent model for smart beams with partially debonded piezoelectric actuator/sensor patches is presented to analyze the effect of the actuator debonding on both open loop and closed loop behaviors. To properly model the short debonded part of the actuator in the debonding region, both moment inertia and transverse shear effect are taken into account. Both displacement continuity and force balance are guaranteed by imposing continuity conditions at the interfaces between the debonded and perfectly bonded regions. The eigenvalue problem for the actively controlled beam with partially debonded actuator patches is derived. The effect of the actuator debonding on the modal shapes is investigated through an example, and the additional modal shapes induced by the debonding are also examined. Furthermore, a scheme of restoring the debonding degenerated active control is given based on real-time frequency updating in the controller, and both theoretical and experimental investigation on the control restoration are carried out. Comparison with the full model and the experiment shows that the equivalent model is effective for beams controlled by debonded piezoelectric actuators and sensors.

1. Introduction

Piezoelectric materials have been widely used as distributed actuators and sensors in vibration and shape control of flexible structures. Some newly developed piezoelectric materials, such as ferroelectric single crystal, can generate much larger strain under very high actuating voltage and have good strain–voltage linearity, and hence, more effective active control can be performed using such high performance materials. However, the large actuating strain of a piezoelectric

*Corresponding author. Fax: +61-2-935-14-841.
E-mail address: ltong@aeromech.usyd.edu.au (L. Tong).

0022-460X/$ - see front matter © 2003 Elsevier Ltd. All rights reserved.
doi:10.1016/j.jsv.2003.08.018

actuator and very high impulse voltage will inevitably increase the chance of delamination of embedded actuator layers or debonding of surface adhered actuator patches from their host structures. When a debonding in a piezoelectric actuator or sensor patch occurs during an active control process, it will significantly affect the control efficiency or may even cause unexpected control failure in the controlled structures. Since actively controlled structures are much more vulnerable to actuator/sensor debonding than uncontrolled ones, it is important to investigate the effects of actuator/sensor debonding on the active control and find the ways of best restoring the originally designed closed loop control.

In recent years, studies on the delaminations in ordinary composite structures have been widely carried out, and damage detection of composite structures using piezoelectric sensors has also attracted an increasing attention [1–3]. However, only a very limited literature can be found on dynamics and vibration control of actively controlled structures with debonded piezoelectric actuators/sensors. Chattopadhyay et al. [4] developed a refined higher-order-theory-based finite element model for dynamics of delaminated smart composite plates. Seely and Chattopadhyay [5] studied the issue of the piezoelectric actuator debonding in a composite beam by using the finite element method (FEM) based on a refined higher order theory. The continuity conditions between the debonded and the non-debonded regions were imposed and implemented using a penalty approach in their finite element model. Youn et al. [6] also experimentally investigated the adaptive control, the variations in natural frequencies and actuation characteristics of composite specimens with actuator delaminations using a neural network controller. Tylikowski [7] presented a bending-extensional model of a simply supported laminated beam with debonded piezoelectric actuator elements, in which the edge delamination is modelled by changing the effective length of the debonded actuator. Recently, Sun and Tong [8] developed a full model of beams with partially debonded piezoelectric sensors/actuators. In this full model, all the layers including the sensor, the actuator, the host beam and even the thin bonding layers are modelled in detail, and both longitudinal and transverse vibrations are considered using classical beam theory and Timoshenko's beam theory [9]. The debonding of the piezoelectric actuator is modelled by assuming that there is no shear and peel stresses in the bonding layer between the actuator and the host structure in the debonding region. Based on this full model, they investigated the effect of debonding of the piezoelectric sensor/actuator on closed loop vibration control. They also presented a scheme for control stability analysis of beams with debonded piezoelectric actuator layers [9].

Although the full model can give good results for dynamic response of both controlled and uncontrolled beams with debonded piezoelectric actuator/sensors, it is time-consuming particularly for the beams with many piezoelectric patches. As a trade off between the accuracy and the computational effort, an equivalent model of beams controlled by debonded actuator and sensor patches are given based on the classical laminate theory in this paper. In this equivalent model, the composite beam segments with perfectly bonded actuators and/or sensors are treated as single equivalent beam segments. The displacement continuity conditions and force balance conditions at the interfaces between different composite beam segments are imposed. A solution scheme for the derived boundary problem is given, and the corresponding eigenvalue problem is derived for the closed loop controlled beam. A method of restoring the active control that has been deteriorated by the system change is demonstrated both theoretically and experimentally.

2. Equivalent model

2.1. Governing equations

Consider a beam attached with piezoelectric actuator sensor patches, as shown in Fig. 1. The left piezoelectric patch pair serves as an actuator pair, and the right pair as sensors. Without losing generality, an edge debonding is introduced at the left end of the upper actuator patch. It is assumed that the adhesive layers used to bond the piezoelectric patches are very thin so that their effects on the stiffness and mass of the composite beam can be negligible. The debonding between the piezoelectric actuator and the host beam is assumed to be throughout the width of the beam, and the contact and fraction between them are not considered for the sake of simplicity.

The whole composite beam contains several different portions such as the host beam segments, the beam with debonded piezoelectric patches, and the segments with perfectly bonded piezo-patches. For different segments, their governing equations have different forms. The governing equations will be given in segments.

For the portions containing the host beam and two perfectly bonded piezoelectric actuator layers on its both surfaces (e. g. BC segment in Fig. 1), employing the Timoshenko's beam theory, the equations of motion can be derived as follows

$$\begin{aligned} \rho_a u_{a,tt} &= T_{a,x} + f_l(x,t), \\ \rho_a w_{a,tt} &= Q_{a,x} + f_t(x,t), \\ J_a \psi_{a,tt} &= M_{a,x} - Q_a, \end{aligned} \tag{1}$$

where the subscript a represents the beam with two perfectly bonded actuator layers, T, Q and M are the stress and moment resultants, respectively, $f_l(x,t)$ and $f_t(x,t)$ are the longitudinal and transverse loads, u and w are the longitudinal and transverse displacements, ψ is the rotation angle of the line element originally perpendicular to the longitudinal axis, ρ_a is the mass density for a unit length, and J_a is the moment of inertia, which are given by

$$\rho_a = \sum_{i=1}^{3} \rho_i b h_i, \quad J_a = \frac{b}{3} \sum_{i=1}^{3} \rho_i (z_i^3 - z_{i-1}^3). \tag{2}$$

In Eq. (2), the subscript 1, 2, 3 refer to the upper piezoelectric layer, the host beam and the lower piezoelectric layer respectively, b is the width of the composite beam, ρ_i is the mass density, h_i is the thickness, z_0, z_1, z_2 and z_3 are the z-co-ordinates of the surfaces and interfaces in the composite beam from its neutral plane, as shown in Fig. 2.

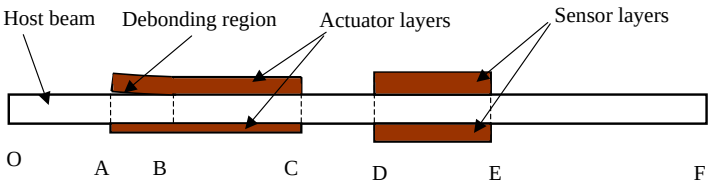

Fig. 1. The beam with debonded piezoelectric actuator/sensor patches.

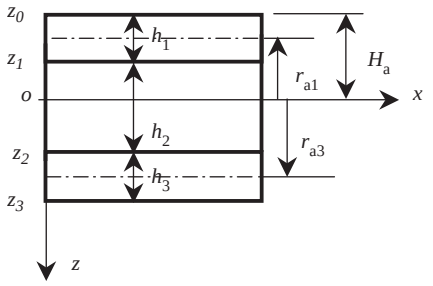

Fig. 2. Notation for a beam bonded with piezoelectric layer.

The rotation angle in Eq. (1) can be expressed as

$$\psi_a = \gamma_a - w_{a,x}, \tag{3}$$

where γ_a is the shear strain at the neutral axis given by

$$\gamma_a = \frac{Q_a}{G_a}, \tag{4}$$

where G_a is the equivalent shear stiffness of the host beam which is dependent on the shape of the cross section and has the following form [10]

$$G_a = \frac{5b}{4}\sum_{i=1}^{3} G_i[(z_i - z_{i-1}) - \frac{4}{3h^2}(z_i^3 - z_{i-1}^3)] \tag{5}$$

in which G_i is the shear modulus, and h is the thickness of the composite beam.

The relationship between the stress resultant, bending moment and the displacements has the form as [11]

$$\begin{aligned} T_a &= A_a u_{a,x} + B_a \psi_{a,x} - be_{311} V(t) - be_{313} V(t), \\ M_a &= B_a u_{a,x} + D_a \psi_{a,x} - be_{311} r_{a1} V(t) - be_{313} r_{a3} V(t), \end{aligned} \tag{6}$$

where e_{311} and e_{313} are the piezoelectric stress constants for the upper and lower actuators respectively, r_{a1} and r_{a3} are the z-co-ordinates of the actuators' mid-planes from the neutral plane of the composite beam, $V(t)$ are the voltage applied on the actuators, A_a, B_a and D_a are the equivalent extension stiffness, extension-bending coupling term and bending stiffness, which are given by

$$A_a = b\sum_{i=1}^{3} E_i h_i, \quad B_a = \frac{1}{2} b \sum_{i=1}^{3} E_i (z_i^2 - z_{i-1}^2), \quad D_a = \frac{b}{3}\sum_{i=1}^{3} E_i (z_i^3 - z_{i-1}^3), \tag{7}$$

where E_i is Young's modulus.

Denoting

$$\begin{aligned} T_a^e &= T_a + be_{311} V(t) + be_{313} V(t), \\ M_a^e &= M_a + be_{311} r_{a1} V(t) + be_{313} r_{a3} V(t), \\ \mathbf{Y}_a(x,t) &= (u_a, T_a^e, w_a, \psi_a, Q_a, M_a^e)^{\mathrm{T}}. \end{aligned} \tag{8}$$

Eqs. (1), (3), (4) and (6) can be combined and written as the following state equation

$$\mathbf{Y}_{a,x} = \mathbf{M}_a \mathbf{Y}_{a,tt} + \mathbf{K}_a \mathbf{Y}_a + \mathbf{F}_a, \quad x_B \leqslant x \leqslant x_C, \tag{9}$$

where

$$\mathbf{M}_a = \begin{bmatrix} 0 & 0 & 0 & 0 & 0 & 0 \\ \rho_a & 0 & 0 & 0 & 0 & 0 \\ 0 & 0 & 0 & 0 & 0 & 0 \\ 0 & 0 & 0 & 0 & 0 & 0 \\ 0 & 0 & \rho_a & 0 & 0 & 0 \\ 0 & 0 & 0 & J_a & 0 & 0 \end{bmatrix}, \quad \mathbf{K}_a = \begin{bmatrix} 0 & \bar{A}_e & 0 & 0 & 0 & \bar{B}_e \\ 0 & 0 & 0 & 0 & 0 & 0 \\ 0 & 0 & 0 & -1 & \frac{1}{G_a} & 0 \\ 0 & \bar{B}_a & 0 & 0 & 0 & \bar{D}_a \\ 0 & 0 & 0 & 0 & 0 & 0 \\ 0 & 0 & 0 & 0 & 1 & 0 \end{bmatrix}, \quad \mathbf{F}_a = \begin{Bmatrix} 0 \\ -f_l \\ 0 \\ 0 \\ -f_t \\ 0 \end{Bmatrix}, \tag{10}$$

$$\bar{A}_a = \frac{D_a}{A_a D_a - B_a^2}, \quad \bar{B}_a = -\frac{B_a}{A_a D_a - B_a^2}, \quad \bar{D}_a = \frac{A_a}{A_a D_a - B_a^2}.$$

Eq. (10) is the actuator equation of the beam bonded with two actuator layers, which establishes the relationship between the longitudinal and transverse vibrations and the voltage applied on the actuators. In the following discussion, only the electric load is considered, and the mechanical load $\mathbf{F}_a$ is zero.

The beam bonded with piezoelectric sensor patches on its upper and lower surfaces (e. g. DE segment in Fig. 1) has the same equations as in Eq. (9) except that the voltage applied on the sensor patches is zero, namely

$$\mathbf{Y}_{s,x} = \mathbf{M}_s \mathbf{Y}_{s,tt} + \mathbf{K}_s \mathbf{Y}_s, \quad x_D \leqslant x \leqslant x_E \tag{11}$$

where $\mathbf{Y}_s = (u_s, T_s, w_s, \psi_s, Q_s, M_s)^{\mathrm{T}}$ and the $\mathbf{M}_s$ and $\mathbf{K}_s$ can be obtained by simply replacing the subscript a with s in Eq. (10).

The equations of motion of the host beam itself (e. g. OA, CD and EF segments in Fig. 1) also have the same form as in Eq. (9), i.e.

$$\mathbf{Y}_{h,x} = \mathbf{M}_h \mathbf{Y}_{h,tt} + \mathbf{K}_h \mathbf{Y}_h, \quad 0 \leqslant x \leqslant x_A, x_C \leqslant x \leqslant x_D, x_E \leqslant x \leqslant x_F \tag{12}$$

where $\mathbf{Y}_h = (u_h, T_h, w_h, \psi_h, Q_h, M_h)^{\mathrm{T}}$, $\mathbf{M}_h$ and $\mathbf{K}_h$ can be obtained by letting

$$\rho_a = \rho_2 b h_2, \quad J_a = \rho_2 b h_2^3/12, \quad G_a = \tfrac{5}{6} G_2 b h_2, \quad V(t) = 0 \tag{13}$$

in Eq. (10).

For the debonding part (AB segment in Fig. 1), the debonded actuator and the beam bonded with only one actuator layer vibrate independently according to the assumption. The governing equations of this part are given as follows.

$$\rho_1 bh_1 u_{1,tt} = T_{1,x}, \quad \rho_1 bh_1 w_{1,tt} = Q_{1,x}, \quad \rho_1 J_1 \psi_{1,tt} = M_{1,x} - Q_1,$$
$$w_{1,x} = \frac{6Q_1}{5G_1 bh_1} - \psi_1, \quad T_1 = E_1 bh_1 u_{1,x} - be_{311} V(t), \quad M_1 = E_1 J_1 \psi_{1,x},$$
$$\rho_d u_{d,tt} = T_{d,x}, \quad \rho_d w_{d,tt} = Q_{d,x}, \quad J_d \psi_{d,tt} = M_{d,x} - Q_d,$$
$$w_{d,x} = \frac{Q_d}{G_d} - \psi_d, \quad T_d = A_d u_{d,x} + B_d \psi_{d,x} - be_{313} V(t),$$
$$M_d = B_d u_{d,x} + D_d \psi_{d,x} - be_{313} r_{ad} V(t), \tag{14}$$

where the subscript d represents the composite beam composed of two laminates, namely, the host beam and the lower actuator layer, r_{ad} is the z-co-ordinates of the mid-plane of the lower actuator layer from the neutral plane of this two layer composite beam. When denoting

$$T_1^e = T_1 + be_{311} V(t), \quad T_d^e = T_d + be_{313} V(t), \quad M_d^e = M_d + be_{313} r_{ad} V(t),$$
$$\mathbf{Y}_1 = (u_1, T_1^e, w_1, \psi_1, Q_1, M_1)^{\mathrm{T}}, \quad \mathbf{Y}_d = (u_d, T_d^e, w_d, \psi_d, Q_d, M_d^e)^{\mathrm{T}}, \quad \mathbf{Y}_D = (\mathbf{Y}_1^{\mathrm{T}}, \mathbf{Y}_d^{\mathrm{T}})^{\mathrm{T}}. \tag{15}$$

Eq. (14) can be written in the following compact form

$$\mathbf{Y}_{D,x} = \mathbf{M}_D \mathbf{Y}_{D,tt} + \mathbf{K}_D \mathbf{Y}_D, \tag{16}$$

where

$$\mathbf{M}_D = \begin{bmatrix} \mathbf{M}_1 & \mathbf{0} \\ \mathbf{0} & \mathbf{M}_d \end{bmatrix}, \quad \mathbf{K}_D = \begin{bmatrix} \mathbf{K}_1 & \mathbf{0} \\ \mathbf{0} & \mathbf{K}_d \end{bmatrix}$$

$$\mathbf{M}_1 = \begin{bmatrix} 0 & 0 & 0 & 0 & 0 & 0 \\ \rho_1 bh_1 & 0 & 0 & 0 & 0 & 0 \\ 0 & 0 & 0 & 0 & 0 & 0 \\ 0 & 0 & 0 & 0 & 0 & 0 \\ 0 & 0 & \rho_1 bh_1 & 0 & 0 & 0 \\ 0 & 0 & 0 & \rho_1 J_1 & 0 & 0 \end{bmatrix}, \quad \mathbf{K}_1 = \begin{bmatrix} 0 & 1/E_1 bh_1 & 0 & 0 & 0 & 0 \\ 0 & 0 & 0 & 0 & 0 & 0 \\ 0 & 0 & 0 & -1 & \frac{6}{5G_1 bh_1} & 0 \\ 0 & 0 & 0 & 0 & 0 & 1/E_1 J_1 \\ 0 & 0 & 0 & 0 & 0 & 0 \\ 0 & 0 & 0 & 0 & 1 & 0 \end{bmatrix}, \tag{17}$$

$$\mathbf{M}_d = \begin{bmatrix} 0 & 0 & 0 & 0 & 0 & 0 \\ \rho_d & 0 & 0 & 0 & 0 & 0 \\ 0 & 0 & 0 & 0 & 0 & 0 \\ 0 & 0 & 0 & 0 & 0 & 0 \\ 0 & 0 & \rho_d & 0 & 0 & 0 \\ 0 & 0 & 0 & 0 & J_d & 0 \end{bmatrix}, \quad \mathbf{K}_d = \begin{bmatrix} 0 & \bar{A}_d & 0 & 0 & 0 & \bar{B}_d \\ 0 & 0 & 0 & 0 & 0 & 0 \\ 0 & 0 & 0 & -1 & 1/G_d & 0 \\ 0 & \bar{B}_d & 0 & 0 & 0 & \bar{D}_d \\ 0 & 0 & 0 & 0 & 0 & 0 \\ 0 & 0 & 0 & 0 & 1 & 0 \end{bmatrix},$$

where the equivalent parameters $\rho_d, J_d, G_d, \bar{A}_d, \bar{B}_d$ and $\bar{D}_d$ can be obtained by similar procedure as in the composite beam composed of three laminates.

2.2. Continuity and boundary conditions

Since each part containing several layers in the beam are treated as a single composite beam segment, the continuity conditions at the interfaces between different composite beam segments should be imposed to keep the displacement continuity and the force balance. There are five such interfaces at A, B, C, D and E, respectively, in the beam shown in Fig. 1.

Interface A:

As shown in Fig. 3, the following equations at the interface A should be imposed:

$$\begin{aligned} &u_A^+ = u_A^- - r_A\psi_A^-, \quad T_A^+ = T_A^-, \quad w_A^+ = w_A^-, \\ &\psi_A^+ = \psi_A^-, \quad Q_A^+ = Q_A^-, \quad M_A^+ = M_A^- + r_A T_A^-, \end{aligned} \tag{18}$$

where

$$r_A = h_1/2 - h_d, \quad h_d = \frac{E_2h_2^2 + E_3h_3^2 + 2E_3h_2h_3}{2(E_2h_2 + E_3h_3)}, \tag{19}$$

where r_A and h_d are shown in Fig. 3b.

Noting the relationship between the T_d^e and T_d, M_d^e and M_d, Eq. (18) can be rearranged as

$$\mathbf{C}_A^-\mathbf{Y}_A^- + \mathbf{C}_A^+\mathbf{Y}_A^+ + \mathbf{F}_A V(t) = 0, \tag{18′}$$

where

$$\mathbf{C}_A^- = \begin{bmatrix} 1 & 0 & 0 & -r_A & 0 & 0 \\ 0 & 1 & 0 & 0 & 0 & 0 \\ 0 & 0 & 1 & 0 & 0 & 0 \\ 0 & 0 & 0 & 1 & 0 & 0 \\ 0 & 0 & 0 & 0 & 1 & 0 \\ 0 & r_A & 0 & 0 & 0 & 1 \end{bmatrix}, \quad \mathbf{C}_A^+ = -\mathbf{I}_6 = -\begin{bmatrix} 1 & 0 & 0 & 0 & 0 & 0 \\ 0 & 1 & 0 & 0 & 0 & 0 \\ 0 & 0 & 1 & 0 & 0 & 0 \\ 0 & 0 & 0 & 1 & 0 & 0 \\ 0 & 0 & 0 & 0 & 1 & 0 \\ 0 & 0 & 0 & 0 & 0 & 1 \end{bmatrix},$$

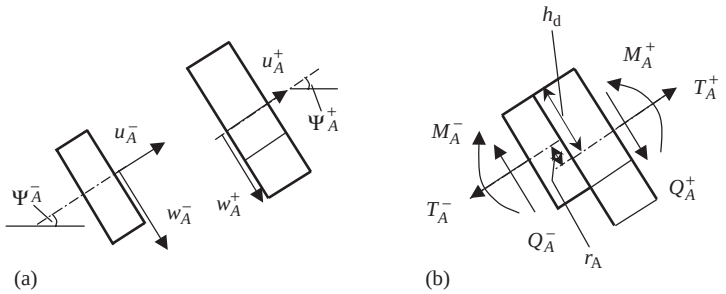

Fig. 3. Continuity conditions at interface A: (a) displacements and (b) forces.

$$\mathbf{F}_A = \begin{Bmatrix} 0 \\ be_{313} \\ 0 \\ 0 \\ 0 \\ be_{313} r_{ad} \end{Bmatrix}, \quad \mathbf{Y}_A^- = \mathbf{Y}_{hA} = \mathbf{Y}_h(x_A), \quad \mathbf{Y}_A^+ = \mathbf{Y}_{dA} = \mathbf{Y}_d(x_A). \tag{20}$$

Interface B:

This is the interface between the debonded and perfectly bonded regions, at which the following nine continuity conditions should be applied (see Fig. 4).

$$\begin{aligned} &u_B^+ = u_{B1}^- - r_{B1}\psi_B^-, \quad u_B^+ = u_{B2}^- - r_{B2}\psi_B^-, \quad T_B^+ = T_{B1}^- + T_{B2}^-, \\ &w_B^+ = w_{B1}^-, \quad w_B^+ = w_{B2}^-, \quad \psi_B^+ = \psi_{b1}^-, \quad \psi_B^+ = \psi_{B2}^-, \\ &Q_B^+ = Q_{B1}^- + Q_{B2}^-, \quad M_B^+ = M_{B1}^- + M_{B2}^- + r_{B1}T_{B1}^- + r_{B2}T_{B2}^-, \end{aligned} \tag{21}$$

where

$$\begin{aligned} &r_{B1} = h_1/2 - ha, \qquad r_{B2} = h_d + h_1 - h_a, \\ &h_a = \frac{E_1h_1^2 + E_2h_2^2 + E_3h_3^2 + 2E_2h_1h_2 + 2E_3h_1h_3 + 2E_3h_2h_3}{2(E_1h_1 + E_2h_2 + E_3h_3)}, \end{aligned} \tag{22}$$

where r_{B1}, r_{B2} and h_a are shown in Fig. 4b.

Eq. (21) can also be written into the matrix form as

$$\mathbf{C}_B^-\mathbf{Y}_B^- + \mathbf{C}_B^+\mathbf{Y}_B^+ + \mathbf{F}_B V(t) = 0, \tag{21′}$$

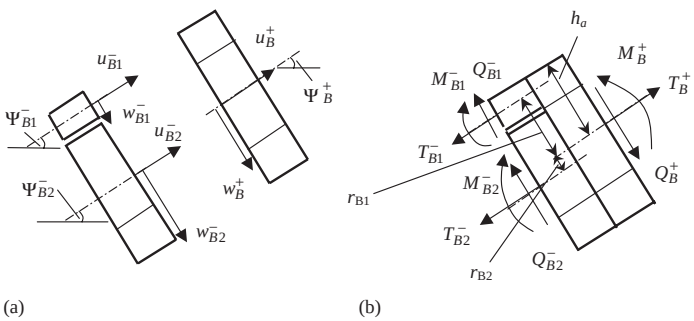

Fig. 4. Continuity conditions at interface B: (a) displacements and (b) forces.

where

$$\mathbf{C}_B^- = \begin{bmatrix} 1 & 0 & 0 & -r_{B1} & 0 & 0 & 0 & 0 & 0 & 0 & 0 & 0 \\ 0 & 0 & 0 & 0 & 0 & 0 & 1 & 0 & 0 & -r_{B2} & 0 & 0 \\ 0 & 1 & 0 & 0 & 0 & 0 & 0 & 1 & 0 & 0 & 0 & 0 \\ 0 & 0 & 1 & 0 & 0 & 0 & 0 & 0 & 0 & 0 & 0 & 0 \\ 0 & 0 & 0 & 0 & 0 & 0 & 0 & 0 & 1 & 0 & 0 & 0 \\ 0 & 0 & 0 & 1 & 0 & 0 & 0 & 0 & 0 & 0 & 0 & 0 \\ 0 & 0 & 0 & 0 & 0 & 0 & 0 & 0 & 0 & 1 & 0 & 0 \\ 0 & 0 & 0 & 0 & 1 & 0 & 0 & 0 & 0 & 0 & 1 & 0 \\ 0 & r_{B1} & 0 & 0 & 0 & 0 & 0 & r_{B2} & 0 & 0 & 0 & 0 \end{bmatrix},$$

$$\mathbf{C}_B^+ = \begin{bmatrix} -1 & 0 & 0 & 0 & 0 & 0 \\ -1 & 0 & 0 & 0 & 0 & 0 \\ 0 & -1 & 0 & 0 & 0 & 0 \\ 0 & 0 & -1 & 0 & 0 & 0 \\ 0 & 0 & -1 & 0 & 0 & 0 \\ 0 & 0 & 0 & -1 & 0 & 0 \\ 0 & 0 & 0 & -1 & 0 & 0 \\ 0 & 0 & 0 & 0 & -1 & 0 \\ 0 & 0 & 0 & 0 & 0 & -1 \end{bmatrix},$$

$$\mathbf{F}_B = (0, \quad 0, \quad 0, \quad 0, \quad 0, \quad 0, \quad 0, \quad 0, \quad be_{311}r_{a3} + be_{313}r_{a3} - be_{313}r_{ad} - be_{311}r_{B1} - be_{313}r_{B2})^{\mathrm{T}}$$

$$\mathbf{Y}_B^- = \mathbf{Y}_{DB} = \mathbf{Y}_D(x_B), \mathbf{Y}_B^+ = \mathbf{Y}_{aB} = \mathbf{Y}_a(x_B). \tag{23}$$

Interface C:

The six continuity conditions at interface C can be expressed as

$$\mathbf{C}_C^- \mathbf{Y}_C^- + \mathbf{C}_C^+ \mathbf{Y}_C^+ + \mathbf{F}_C V(t) = 0, \tag{24}$$

where

$$\mathbf{C}_C^- = \begin{bmatrix} 1 & 0 & 0 & -r_C & 0 & 0 \\ 0 & 1 & 0 & 0 & 0 & 0 \\ 0 & 0 & 1 & 0 & 0 & 0 \\ 0 & 0 & 0 & 1 & 0 & 0 \\ 0 & 0 & 0 & 0 & 1 & 0 \\ 0 & r_C & 0 & 0 & 0 & 1 \end{bmatrix}, \quad \mathbf{C}_C^+ = -\mathbf{I}_6, \quad \mathbf{F}_C = -b \begin{Bmatrix} 0 \\ e_{311} + e_{313} \\ 0 \\ 0 \\ 0 \\ e_{311}r_{a1} + e_{313}r_{a3} + e_{311}r_C + e_{313}r_C \end{Bmatrix},$$

$$\mathbf{Y}_C^- = \mathbf{Y}_{aC} = \mathbf{Y}_a(x_C), \quad \mathbf{Y}_C^+ = \mathbf{Y}_{hC} = \mathbf{Y}_h(x_C), \quad r_C = h_a - h_1 - h_2/2. \tag{25}$$

Similarly, the continuity conditions at interfaces D and E can be expressed as

$$\begin{aligned} \mathbf{C}_D^- \mathbf{Y}_D^- + \mathbf{C}_D^+ \mathbf{Y}_D^+ = 0, \quad \text{at } x = x_D \\ \mathbf{C}_E^- \mathbf{Y}_E^- + \mathbf{C}_E^+ \mathbf{Y}_E^+ = 0, \quad \text{at } x = x_E \end{aligned} \tag{26}$$

Note that there is no control voltage related items in the continuity conditions of the sensor patches.

Boundary conditions:

The boundary conditions at both ends of the host beam can be expressed in the following general form

$$\mathbf{P}_1 \mathbf{Y}_h(0) + \mathbf{P}_2 \mathbf{Y}_h(x_F) = \mathbf{P}_0, \quad \text{at } x = 0 \text{ and } x = x_F, \tag{27}$$

where $\mathbf{P}_1 \in R^{6\times 6}$ and $\mathbf{P}_2 \in R^{6\times 6}$ are matrices related to the boundary conditions, and $\mathbf{P}_0 \in R^6$ is a vector composed of the designated displacements and forces at the beam's ends. In addition, the boundary conditions of the left end of the debonded actuator can be written as

$$\mathbf{P}_d \mathbf{Y}_1(x_A) = \mathbf{P}_{d0} V(t), \quad \text{at } x = x_A \tag{28}$$

where $\mathbf{P}_d \in R^{3\times 6}$ and $\mathbf{P}_{d0} \in R^3$ depends on the constraint at the end of the piezoelectric actuator patch. When the debonded end of the actuator is free,

$$\mathbf{P}_d = \begin{bmatrix} 0 & 1 & 0 & 0 & 0 & 0 \\ 0 & 0 & 0 & 0 & 1 & 0 \\ 0 & 0 & 0 & 0 & 0 & 1 \end{bmatrix}, \quad \mathbf{P}_{d0} = \begin{Bmatrix} -be_{311} \\ 0 \\ 0 \end{Bmatrix} \tag{29}$$

2.3. Sensor equation and control law

When the piezoelectric patch is used as a distributed sensor, its charge output can be derived as [11]

$$q(t) = be_{31s} \int_{x_D}^{x_E} (u_{s,x} + r_s \psi_{s,x}) \, \mathrm{d}x, \tag{30}$$

where r_s is the z-co-ordinate of the mid-plane of the sensor patch from the neutral plane of the composite beam. When the thickness for each layer in the laminated beam is constant, Eq. (30) can be simplified as

$$q(t) = be_{31s}[u_s(x_E) - u_s(x_D)] + be_{31s} r_s [\psi_s(x_E) - \psi_s(x_D)] \tag{31}$$

In closed loop control, the voltage applied on the piezoelectric actuators is designed as a function of the sensor output signal according to some control laws. In order to control the first several modes of the composite beam, employ the modal velocity observers (MVOs) for the nth target mode as follows [12]

$$\begin{aligned} &\xi_{n,tt}(t) + 2\omega_{cn}\zeta_{1n}\xi_{n,t}(t) + \omega_{cn}^2 \xi_n(t) = \omega_{cn}^2 q(t), \\ &\eta_{n,tt}(t) + 2\omega_{cn}\zeta_{2n}\eta_{n,t}(t) + \omega_{cn}^2 \eta_n(t) = \omega_{cn}\dot{\eta}_{n,t}(t), \end{aligned} \quad n = 1, 2, \ldots, N \tag{32}$$

where ω_{cn} is the natural frequency of the observer, ζ_{1n} and ζ_{2n} are the damping ratios which can be adjusted to make the closed loop control more robust, and N is the number of the modes to be controlled. When the natural frequency of the modal velocity observer ω_{cn} coincides with one of

the modal frequencies of the composite beam, the output $\eta_n(t)$ of the observer will be 180° out of phase with the target modal velocity, and hence, the modal velocity of the target mode can be measured. Therefore, using the MVO, the modal frequencies of the modes to be controlled should be measured or estimated before the control is performed so that the output of the MVO can be made as close as possible to the real modal velocity.

To control the first N modes of the beam, the control voltage is designed as

$$V(t) = \sum_{n=1}^{N} g_n \eta_n(t), \tag{33}$$

where g_n is the control gain for the nth mode. Eqs. (32) and (33) give a practical control scheme, which is called MVO controller.

In general, due to the error of the measured or estimated frequencies, the observed modal velocity will not be exactly in phase with the real one, and consequently, it will affect the control efficiency and may even destabilize the control. In this case, the phase difference between the observed and real modal velocity highly depends on the damping ratios ζ_{n1} and ζ_{n2}. When the damping ratios are very small, even a slight error of the observer frequency will result in a significant phase difference between the observed velocity and the real one. On the contrary, when the damping ratios of the MVO are larger, the phase distortion of the observed modal velocity will not be sensitive to the error of the measured frequency. Therefore, for the purpose of robust control, there are two ways to increase the control robustness. One is to use proper damping ratios in the MVO, another is to use the frequency as accurate as possible. It is known that debonding of a piezoelectric patch will lead a frequency change, if the frequency used in the MVO controller is updated adaptively as debonding develops, the control will be still effective.

3. Solution method

To obtain the eigenvalue problem of the beam with partially debonded piezoelectric patches, rewrite the state vectors into the following form

$$\mathbf{Y}_h(x,t) = \bar{\mathbf{Y}}_h(x)e^{\lambda t}, \quad \mathbf{Y}_D(x,t) = \bar{\mathbf{Y}}_D(x)e^{\lambda t}, \quad \mathbf{Y}_a(x,t) = \bar{\mathbf{Y}}_a(x)e^{\lambda t}, \quad \mathbf{Y}_s(x,t) = \bar{\mathbf{Y}}_s(x)e^{\lambda t}, \tag{34}$$

where λ is known as eigenvalue, $\bar{\mathbf{Y}}_h(x), \bar{\mathbf{Y}}_D(x), \bar{\mathbf{Y}}_a(x)$ and $\bar{\mathbf{Y}}_s(x)$ are the eigenfunctions in different beam segments. Substituting Eq. (34) into the governing equations, the partial differential equations can be transformed to ordinary differential equations. For example, the governing equations in Eq. (9) becomes

$$\bar{\mathbf{Y}}_{a,x} = \mathbf{A}_a(\lambda)\bar{\mathbf{Y}}_a, \quad x_B \leqslant x \leqslant x_C \tag{35}$$

where $\mathbf{A}_a(\lambda) \in R^{6\times 6}$ is a matrix with parameter λ.

$$\mathbf{A}_a(\lambda) = \mathbf{M}_a\lambda^2 + \mathbf{K}_a. \tag{36}$$

Eqs. (35) can be solved in terms of transition matrix, and the relationship between the state vectors at x_B and x_C can be expressed as [13]

$$\bar{\mathbf{Y}}_C^- = \mathbf{\Phi}_{BC}(\lambda)\bar{\mathbf{Y}}_B^+ \tag{37}$$

where $\mathbf{\Phi}_{BC}(\lambda)$ is the transition matrix between x_B and x_C which is given by

$$\mathbf{\Phi}_{BC}(\lambda) = \exp[A_a(\lambda)(x_B - x_C)]. \tag{38}$$

Following the same procedure, the equations for each segment of the composite beam can be derived as

$$\begin{aligned}
\bar{\mathbf{Y}}_A^- &= \mathbf{\Phi}_{AO}(\lambda)\bar{\mathbf{Y}}_O,\\
\bar{\mathbf{Y}}_B^- &= \mathbf{\Phi}_{BA}(\lambda)\bar{\mathbf{Y}}_A^+,\\
\bar{\mathbf{Y}}_C^- &= \mathbf{\Phi}_{CB}(\lambda)\bar{\mathbf{Y}}_B^+,\\
\bar{\mathbf{Y}}_D^- &= \mathbf{\Phi}_{DC}(\lambda)\bar{\mathbf{Y}}_C^+,\\
\bar{\mathbf{Y}}_E^- &= \mathbf{\Phi}_{ED}(\lambda)\bar{\mathbf{Y}}_D^+,\\
\bar{\mathbf{Y}}_F &= \mathbf{\Phi}_{FE}(\lambda)\bar{\mathbf{Y}}_E^+.
\end{aligned} \tag{39}$$

Substituting Eq. (34) into the continuity and boundary conditions, yields

$$\begin{aligned}
&\mathbf{C}_A^-\bar{\mathbf{Y}}_A^- + \mathbf{C}_A^+\bar{\mathbf{Y}}_A^+ + \mathbf{F}_A\bar{V} = 0, && \text{at } x = x_A\\
&\mathbf{C}_B^-\bar{\mathbf{Y}}_B^- + \mathbf{C}_B^+\bar{\mathbf{Y}}_B^+ + \mathbf{F}_B\bar{V} = 0, && \text{at } x = x_B\\
&\mathbf{C}_C^-\bar{\mathbf{Y}}_C^- + \mathbf{C}_A^+\bar{\mathbf{Y}}_A^+ + \mathbf{F}_C\bar{V} = 0, && \text{at } x = x_C\\
&\mathbf{C}_D^-\bar{\mathbf{Y}}_A^- + \mathbf{C}_D^+\bar{\mathbf{Y}}_A^+ = 0, && \text{at } x = x_D\\
&\mathbf{C}_E^-\bar{\mathbf{Y}}_E^- + \mathbf{C}_E^+\bar{\mathbf{Y}}_E^+ = 0, && \text{at } x = x_E\\
&\mathbf{P}_d\bar{\mathbf{Y}}_1(x_A) = \mathbf{P}_{d0}\bar{V}, && \text{at } x = x_A\\
&\mathbf{P}_1\mathbf{Y}_h(0) + \mathbf{P}_2\mathbf{Y}_h(x_F) = 0, && \text{at } x = 0 \text{ and } x = x_F
\end{aligned} \tag{40}$$

where $\bar{V}$ can be expressed as follow according to the control law in Eq. (33) and the sensor Eq. (31).

$$\begin{aligned}
&\bar{V} = \mathbf{G}(\bar{\mathbf{Y}}_E^- - \bar{\mathbf{Y}}_D^+),\\
&\mathbf{G} = be_{31s}H(\lambda)[\,1 \quad 0 \quad 0 \quad r_s \quad 0 \quad 0\,],\\
&H(\lambda) = \sum_{n=1}^{N} \frac{\omega_{cn}^3\lambda}{(\lambda^2 + 2w_{cn}\zeta_{1n}\lambda + \omega_{cn}^2)(\lambda^2 + 2w_{cn}\zeta_{2n}\lambda + \omega_{cn}^2)}.
\end{aligned} \tag{41}$$

Inserting Eq. (41) into Eq. (40), Eq. (39) together with Eq. (40) can be written into the following matrix form

$$\mathbf{R}(\lambda)\mathbf{Z} = 0, \tag{42}$$

where

$$\mathbf{R}(\lambda)=\begin{bmatrix}
\boldsymbol{\Phi}_{AO} & -\mathbf{I}_6 & \mathbf{0} & \mathbf{0} & \mathbf{0} & \mathbf{0} & \mathbf{0} & \mathbf{0} & \mathbf{0} & \mathbf{0} & \mathbf{0} & \mathbf{0} & \mathbf{0} & \mathbf{0} \\
\mathbf{0} & \mathbf{0} & \boldsymbol{\Phi}_{BA} & & -\mathbf{I}_{12} & & \mathbf{0} & \mathbf{0} & \mathbf{0} & \mathbf{0} & \mathbf{0} & \mathbf{0} & \mathbf{0} & \mathbf{0} \\
\mathbf{0} & \mathbf{0} & \mathbf{0} & \mathbf{0} & \mathbf{0} & \mathbf{0} & \boldsymbol{\Phi}_{CB} & -\mathbf{I}_6 & \mathbf{0} & \mathbf{0} & \mathbf{0} & \mathbf{0} & \mathbf{0} & \mathbf{0} \\
\mathbf{0} & \mathbf{0} & \mathbf{0} & \mathbf{0} & \mathbf{0} & \mathbf{0} & \mathbf{0} & \mathbf{0} & \boldsymbol{\Phi}_{DC} & -\mathbf{I}_6 & \mathbf{0} & \mathbf{0} & \mathbf{0} & \mathbf{0} \\
\mathbf{0} & \mathbf{0} & \mathbf{0} & \mathbf{0} & \mathbf{0} & \mathbf{0} & \mathbf{0} & \mathbf{0} & \mathbf{0} & \mathbf{0} & \boldsymbol{\Phi}_{ED} & -\mathbf{I}_6 & \mathbf{0} & \mathbf{0} \\
\mathbf{0} & \mathbf{0} & \mathbf{0} & \mathbf{0} & \mathbf{0} & \mathbf{0} & \mathbf{0} & \mathbf{0} & \mathbf{0} & \mathbf{0} & \mathbf{0} & \mathbf{0} & \boldsymbol{\Phi}_{FE} & -\mathbf{I}_6 \\
\mathbf{0} & \mathbf{C}_A^- & \mathbf{0} & \mathbf{C}_A^+ & \mathbf{0} & \mathbf{0} & \mathbf{0} & \mathbf{0} & \mathbf{0} & \mathbf{0} & -\mathbf{F}_A\mathbf{G} & \mathbf{F}_A\mathbf{G} & \mathbf{0} & \mathbf{0} \\
\mathbf{0} & \mathbf{0} & \mathbf{0} & \mathbf{0} & \mathbf{C}_B^- & \mathbf{C}_B^+ & \mathbf{0} & \mathbf{0} & \mathbf{0} & -\mathbf{F}_B\mathbf{G} & \mathbf{F}_B\mathbf{G} & \mathbf{0} & \mathbf{0} & \\
\mathbf{0} & \mathbf{0} & \mathbf{0} & \mathbf{0} & \mathbf{0} & \mathbf{0} & \mathbf{0} & \mathbf{C}_C^- & \mathbf{C}_C^+ & \mathbf{0} & -\mathbf{F}_C\mathbf{G} & \mathbf{F}_C\mathbf{G} & \mathbf{0} & \mathbf{0} \\
\mathbf{0} & \mathbf{0} & \mathbf{0} & \mathbf{0} & \mathbf{0} & \mathbf{0} & \mathbf{0} & \mathbf{0} & \mathbf{0} & \mathbf{C}_D^- & \mathbf{C}_D^+ & \mathbf{0} & \mathbf{0} & \mathbf{0} \\
\mathbf{0} & \mathbf{0} & \mathbf{0} & \mathbf{0} & \mathbf{0} & \mathbf{0} & \mathbf{0} & \mathbf{0} & \mathbf{0} & \mathbf{0} & \mathbf{0} & \mathbf{C}_E^- & \mathbf{C}_E^+ & \mathbf{0} \\
\mathbf{0} & \mathbf{0} & \mathbf{P}_d & \mathbf{0} & \mathbf{0} & \mathbf{0} & \mathbf{0} & \mathbf{0} & \mathbf{0} & \mathbf{0} & -\mathbf{P}_{d0}\mathbf{G} & \mathbf{P}_{d0}\mathbf{G} & \mathbf{0} & \mathbf{0} \\
\mathbf{P}_1 & \mathbf{0} & \mathbf{0} & \mathbf{0} & \mathbf{0} & \mathbf{0} & \mathbf{0} & \mathbf{0} & \mathbf{0} & \mathbf{0} & \mathbf{0} & \mathbf{0} & \mathbf{0} & \mathbf{P}_2
\end{bmatrix},$$

$$\mathbf{Z}=(\mathbf{Y}_O^{\mathrm{T}},\mathbf{Y}_A^{-\mathrm{T}},\mathbf{Y}_A^{+\mathrm{T}},\mathbf{Y}_B^{-\mathrm{T}},\mathbf{Y}_B^{+\mathrm{T}},\mathbf{Y}_C^{-\mathrm{T}},\mathbf{Y}_C^{+\mathrm{T}},\mathbf{Y}_D^{-\mathrm{T}},\mathbf{Y}_E^{-\mathrm{T}},\mathbf{Y}_E^{+\mathrm{T}},\mathbf{Y}_F^{\mathrm{T}})^{\mathrm{T}}. \tag{43}$$

Eq. (42) gives a complex eigenvalue problem of the beam controlled using partially debonded piezoelectric patches. The eigenvalues of the closed loop system can be obtained by solving the following characteristic equation

$$|\mathbf{R}(\lambda)|=0. \tag{44}$$

Once the eigenvalues are solved from Eq. (44), their corresponding eigenvectors can be obtained from Eq. (42). The eigenfunctions can be constructed in terms of transition matrices as in Eq. (37).

For a controlled beam, its eigenvalues appear as conjugative complex pairs. If all the eigenvalues have negative real parts, the closed loop system is stable. Each eigenvalue corresponds to a vibrations mode, whose real part indicates the active modal damping, and whose imaginary part is the damped frequency for the controlled beam.

4. Examples and experimental investigation

4.1. Comparison with experiment results

To validate the equivalent model, the result obtained by the present model will be compared with those from the experiment and a full model developed by the authors. To this end, the active vibration control experiment of a beam with debonded piezoelectric patches was performed using the MVO controller. The test specimen is a 60 cm × 3 cm × 0.89 mm cantilevered aluminum beam bonded with two pairs of lead zirconate titanate (PZT) patches, as shown in Fig. 5. The left two PZT patch, 1 cm away from the fixed end to their left ends, are used as the actuators, and upper PZT patch out of the right two, 8 cm away from the clamped end to their left ends, is used as the

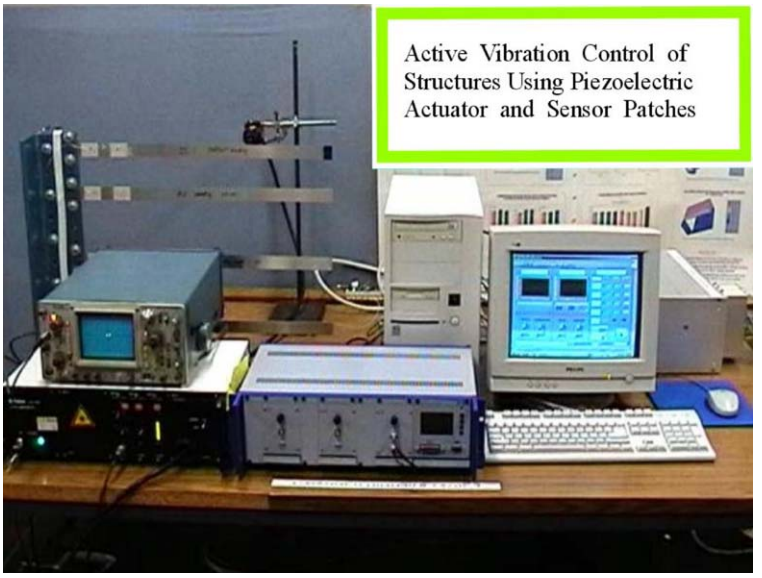

Fig. 5. Experiment setup.

sensor patch. The Young's modulus, mass density and the Poisson ratio of the host beam are 69 GPa, 2700 kg/m^3 and 0.3 respectively. All the four PZT patches have the same geometrical dimensions and material properties except the piezoelectric constants. Young's modulus, mass density and the Poisson ratio of the 4 cm × 3 cm × 0.5 mm PZT patches are 70 GPa, 7600 kg/m^3 and 0.3 respectively. The average piezoelectric stress e_{31} of actuator patches is 9.065 V/m. The piezoelectric stress constant of the sensor patch is 9.8 V/m, and its capacitance is $C_p = 41190$ pF. To investigate the effect of the actuator debonding on the open-loop and closed-loop system, other three specimens, in which an 0.5, 1 and 1.5 cm long edge debondings are introduced, respectively, using a piece of 0.02-mm-thick Teflon film at the left end of the upper actuator patches, are also prepared.

In the experiment, the sensor signal was sampled by a computer with a LabVIEW data acquisition system. A control program was developed based on LabVIEW graphical programming platform. In order to increase the sampling rate, a control kernel was developed using C++ language and integrated with the control program by taking advantage of the code interface node (CIN) function provided by LabVIEW. According to the control law in Eq. (33), the control program generates the control voltage, which, after amplified by a PI E-507.00 HVPZT power amplifier (output range: −550 to 550 V) with gain $g_p = 100$, is fed back to the PZT actuators.

The first two frequencies of specimen with perfectly bonded PZT patches are measured as 2.45 and 13.53 Hz, respectively, which are in good agreement with the theoretical ones shown in Table 1. The natural damping ratios for the first two modes of specimen 1 are measured as 0.0045 and 0.0013, respectively. The first five frequencies obtained by the equivalent model and the full model are also given in Table 1. As shown in Table 1, both equivalent model and the full model can give good estimations for the first five modal frequencies, and the relative errors for the

Table 1
Frequencies of the beam with perfectly bonded PZT patches

Mode no.	Present model		Full model		Experiment
	Frequency (Hz)	Error (%)	Frequency (Hz)	Error (%)	Frequency (Hz)
1	2.499	2	2.469	0.78	2.45
2	14.106	4.26	13.963	3.20	13.53
3	35.510	2.63	35.221	1.79	34.60
4	66.306	2.94	65.824	2.19	64.41
5	110.618	1.97	109.852	1.26	108.48

estimation are less than 4.3%. The theoretical frequencies are higher than those measured from the test. The frequencies calculated from the equivalent model are consistently higher than those from the full model. Table 1 indicates that the full model can provide better estimation for modal frequencies than the equivalent model at the higher cost in computation.

In the closed loop control, the first two modes are controlled. The hardware control gain in the experiment can be determined by $g_h = G_p/C_p = 2.43 \times 10^9$. The real control gain can be easily adjusted by multiplying the hardware gain with different constants in the control program to obtain the desired control effect. To control the first two modes of the four specimens, The measured modal frequencies (2.45 and 13.53 Hz) are used respectively in the modal velocity observers in Eq. (32), and the damping ratios are taken as $\xi_{c1} = 0.6$ and $\xi_{c2} = 0.65$ for the two MVOs. The same control gain, $g = 2.43 \times 10^9$, are used for these two controlled modes. Before controlling each mode, a negative control gain is used to make the controller as an exciter and excite the designed mode. Then switch off the excitation, and change to a positive gain, the active control is turned on to control this mode. Fig. 6 gives the control result for the beam with perfectly bonded actuator patches, and Fig. 7 presents the sensor outputs and the control voltage for the beam with 1 cm edge debonding at the left end of the upper actuator patch. Both Figs. 6 and 7 show that the first two modes are successfully controlled by the MVO controller even in the presence of the actuator debonding. The active damping ratios measured in the experiment for all specimens are listed in Table 2. As a comparison, the theoretical results obtained from the present model and the full model are also given in Table 2.

Table 2 shows that the active damping ratios correlate well to the experiments results, particularly for the first mode. For example, for the four specimens with different lengths of debonding, the damping ratios of the first mode obtained by the present model are 0.0796, 0.0753, 0.0715 and 0.0679 respectively, and those measured in the experiment are 0.072, 0.066, 0.065 and 0.063, the relative errors are 10.6%, 14.1%, 10% and 7.8%, respectively. For the second mode, the theoretical damping ratios calculated from the present equivalent model are larger than the tested ones, and their relative differences are within a range from 37% to 51%. It can be observed from Table 2 that the active damping ratios obtained from the equivalent model are also in agreement with those from the full model, and their relative differences are less than 22%. It is noted that the equivalent model gives larger estimations for both frequencies and damping ratios than the full model in most cases.

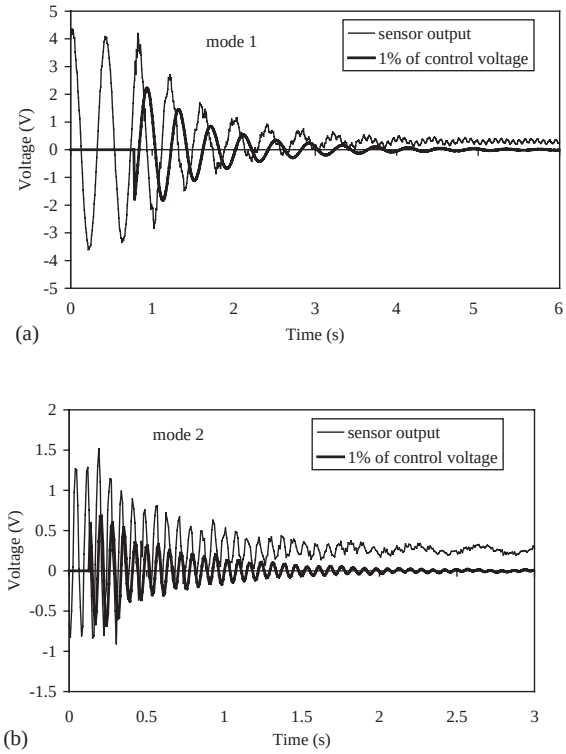

Fig. 6. Time history of the sensor output and the control voltage for beam with perfectly bonded actuators: (a) mode 1 and (b) mode 2.

4.2. Modal shapes of beam with debonded PZT patch

The debonding of the actuator can affect not only the modal frequencies and damping ratios, but also the modal shapes of the beam. To examine the modal shapes of the beam with a 2 cm edge debonding of the actuator, its eigenvalues and the associated eigenfunctions can be solved from Eqs. (44) and (42) respectively. The first four eigenvalues of the open-loop beam are solved as $\pm 15.62I$, $\pm 88.01I$, $\pm 221.64I$ and $\pm 415.10I$, respectively, i.e. the first four modal frequencies are 2.49, 14.00, 35.27 and 66.07 Hz, which are smaller than those of the beam with perfectly bonded actuators. Substituting each eigenvalue into Eq. (42), and normalizing the eigenvector by setting the tip deflection as 1, the eigenvector related to this eigenvalue can be obtained. This eigenvector can give both displacement modal functions and force modal functions because the state vector consists of displacements and internal forces. The first four modal functions for the open loop beam with 2 cm debonded actuator patches are plotted in Fig. 8. It can be seen that the debonded part of the actuator almost has the same transverse displacement with the corresponding part of the host beam for the first four modes, and the differences between them are not noticeable in this case, as shown in Fig. 8(a) and (b). However, the rotation angles of the debonded part of the actuator are quite different from those of the corresponding part of the host beam, as shown in Fig. 8(c) and (d). It is noted that any point of the debonded actuator part has

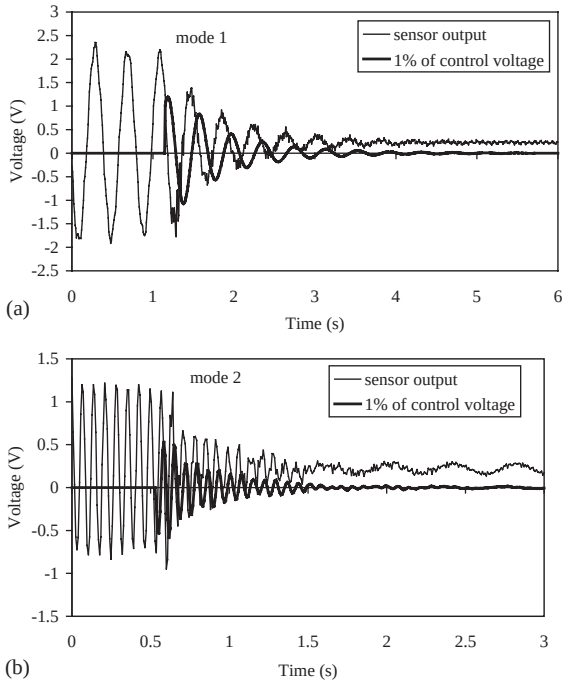

Fig. 7. Time history of the sensor output and the control voltage for beam with 1 cm debonded actuator: (a) mode 1 and (b) mode 2.

Table 2
Comparison of the theoretical active damping ratios with the test ones

Mode no.	Debonding length (cm)	Present model	Full model	Experiment
1	0	0.0796	0.0675	0.072
	0.5	0.0753	0.0640	0.066
	1.0	0.0715	0.0615	0.065
	1.5	0.0679	0.0590	0.063
2	0	0.0385	0.0317	0.028
	0.5	0.0364	0.0288	0.024
	1.0	0.0343	0.0269	0.023
	1.5	0.0324	0.0252	0.022

almost the same rotation angle as the interface point of debonding. Since the modal frequencies for the first four modes of the beam are much lower than the additional frequencies, i.e., the resonance frequencies of the debonded actuator part, its elastic strain is very small and its movement is very close to the rigid movement.

Besides the modes of the original system without actuator debonding, additional modes will be induced by the debonding of the actuator. In this case, the debonded part of the actuator vibrates similar to a beam with an elastic support, and its vibration will be coupled with the original system and results in the additional modes. The frequency for of first additional mode is calculated as

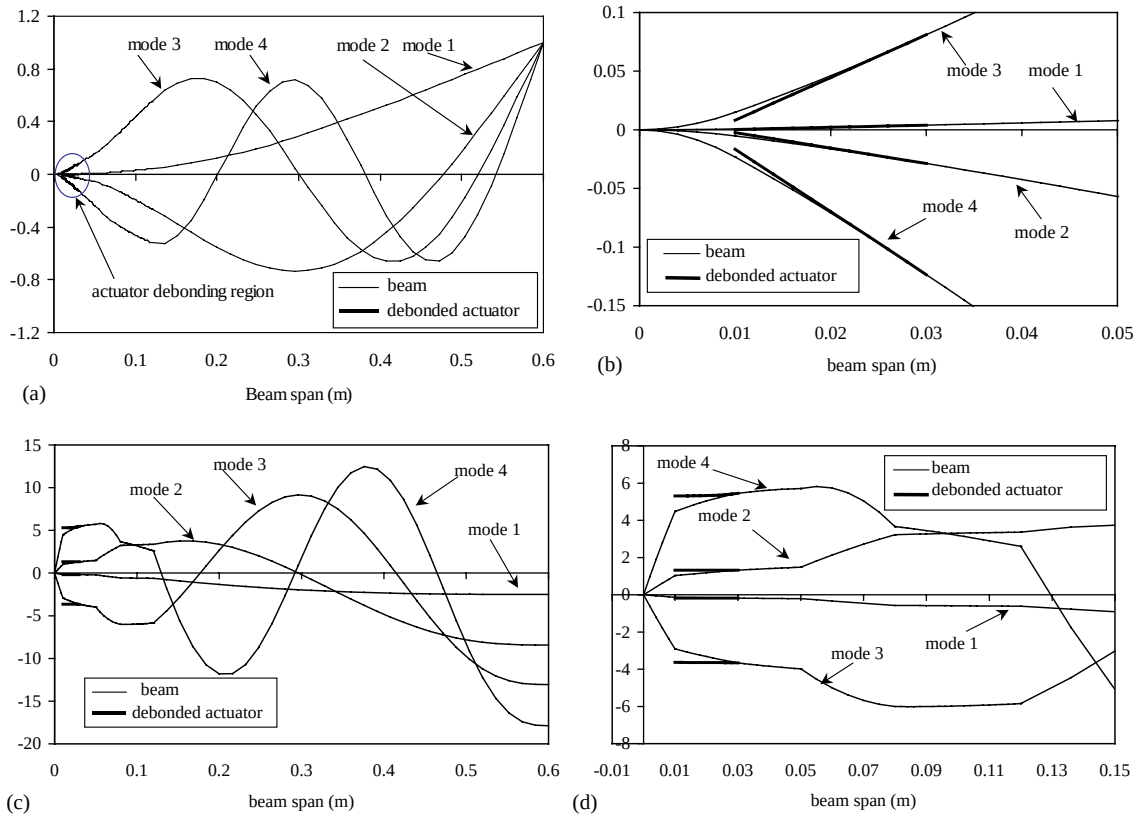

Fig. 8. Modal shapes of the beam with 2 cm edge debonded actuator: (a) modal functions for the first four transverse displacements along the entire beam; (b) modal functions for the first four transverse displacements along the entire beam at the neighborhood of the debonding region; (c) modal functions for the first four rotation angles along the entire beam and (d) modal functions for the first rotation angles along the entire beam at the neighborhood of the debonding region.

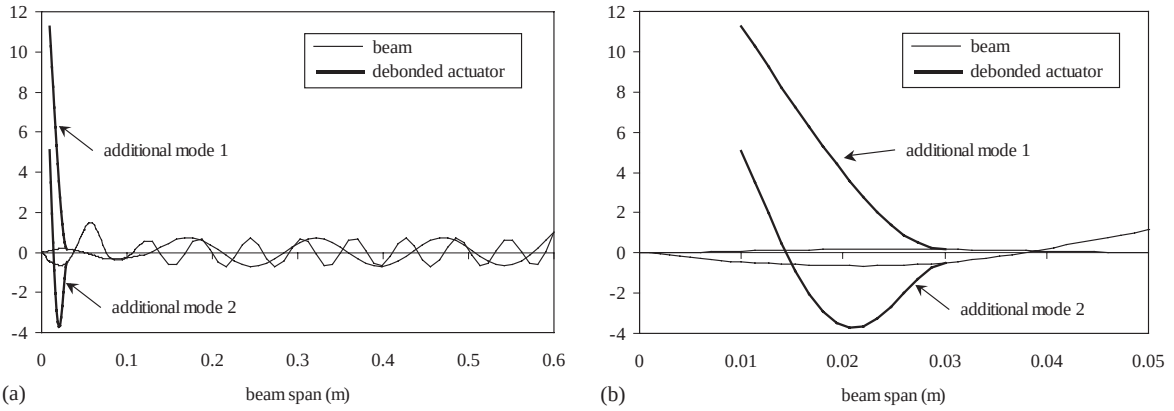

Fig. 9. Additional modal shapes induced by a 2 cm debonding of the actuator: (a) additional modal functions along the entire beam and (b) additional modal functions at the neighborhood of the debonding region.

370.475 Hz, which lies between the 8th (302.3 Hz) and 9th (396.789 Hz) modal frequencies of the original beam without actuator debonding. Fig. 9 gives the modal shape of the first additional modal shape. The frequency of the second additional mode induced by the edge debonding is 2222.9 Hz, and its modal shape is also shown in Fig. 9. As shown in Fig. 9, when the beam vibrates according to these two additional modes, the main vibration part of the beam is the debonded part of actuator only, whereas other parts of the beam almost remain still.

The vibration of the debonded part of the actuator can affects the frequencies and modal shapes of its neighbor modes more remarkably than those of other modes. For example, the first additional mode is inserted between the 8th and 9th mode of the original system and changes their frequencies from their original values to 301.504 and 399.577 Hz, respectively. It also changes the frequency of the lower neighbor mode of the second additional mode from original 1851.34 to 1838.76 Hz and pushes the higher neighbor from original 2193.09 to 2146.09 Hz. In this case, the debonded part of the actuator is deeply involved in its neighbor mode because of the closeness of their frequencies, as shown in Fig. 10. Fig. 10 gives the 10th and 21st modal shapes of the beam with debonded actuator whose frequencies are close to the first two additional modes. As indicated in Fig. 8, unlike the lower modal shapes shown in Fig. 8, the contribution of the debonded part of the actuator to these two mode is significant.

4.3. Control restoration

In the active vibration control, the control effects of the MVO controller depend on two parameters, namely, the frequencies and damping ratios of the MVO. It is well known that debonding of the actuator will change the frequencies of the beam, and consequently affects the control efficiency of the active control and may even destabilize the closed loop control. A natural way to improve the efficiency of the active control is real-time measuring of the frequencies and their updating in the controller. This scheme is expected to best restore the original control of the beam degenerated by a debonding of the PZT actuator. To demonstrate the effect of such scheme, both theoretical and experimental investigations are carried out. In the experiment, since it is hard to change the frequencies quickly using four specimens with different debonding lengths, only the

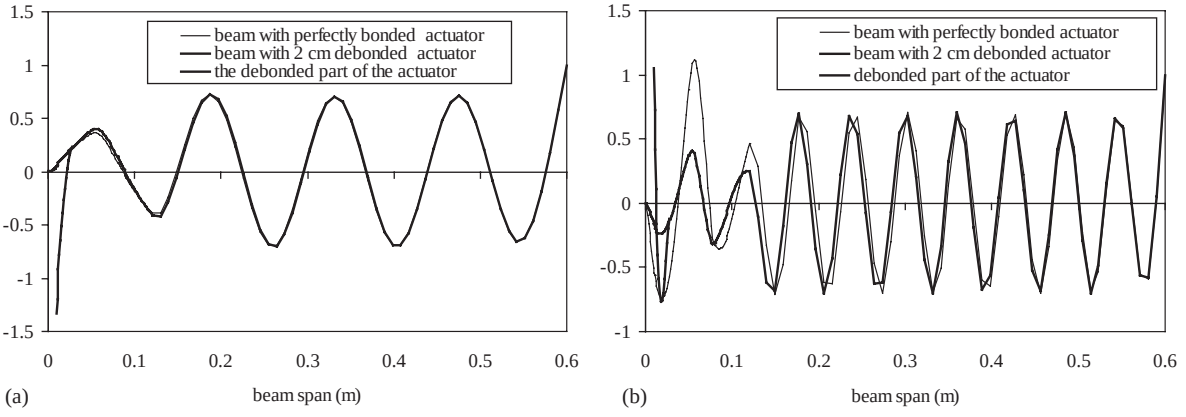

Fig. 10. The modal shapes of neighbor modes of the additional modes: (a) the 10th modal function and (b) the 21st modal function.

specimen with perfectly bonded PZT actuators is used and the frequency change is made by adhering a pair of mass patches with different lengths on its free end.

The attached mass patches are made of the same material as the host beam, and their thickness and width are also identical. Three pairs of mass patches with length of 1, 2 and 3 cm were prepared and were attached each time using double-sided adhesive tape at the free end of the specimen. In order to measure the first several frequencies online, a frequency detection program is added to the control program, in which the power spectrum and the peak detector functions provided by LabVIEW system are employed. Before the active control, a voltage impulse is applied to the actuator patch to excite the beam, and the frequency detection program run simultaneously to measure the frequencies. Then the measured frequencies are input to the MVO controller in control program so that the vibration can be adaptively controlled.

Table 3 lists the first five frequencies of the beam attached with different mass patches measured in the experiment. The frequencies obtained by the equivalent model are also given in Table 3. It can be seen from Table 3 that the theoretical frequencies obtained by the present model are in good agreement with those measured in the experiment, and their relative differences are less than 5.7%. Table 3 also shows that the mass attachment at the free end of the cantilever beam can decrease the modal frequencies of the beam, particularly the first one. For example, a pair of 3 cm mass patches cause a reduction in the fundamental frequencies by 17.1% according to the test data and 16.0% via the theoretical data. It can also decrease the fifth modal frequency by 4.5%.

To investigate the effect of adaptively changing the frequencies in the MVO controller, the first two modes are actively controlled for the specimen with different mass attachments. For each mode of the beam with each kind of mass attachment, the active control was performed twice. At the first time, the frequencies of the original beam (without mass attachment) were used in the MVO controller to control the beam with the mass attachment, and in the second time, the frequencies in the MVO controller were updated to the online detected ones. Fig. 11 presents the time history of both sensor outputs and control voltages in the control process. The active damping ratios provided by the active vibration control can be measured from the time history of either the sensor output or the control voltage, and they are show in Fig. 12. For the purpose of comparison, the theoretical damping ratios obtained by the present equivalent model are also given in Fig. 12. It can be seen that the theoretical damping ratios correlate reasonably well in trend to the measured ones for both vibration modes.

Table 3
Frequencies of the cantilever beam attached with mass patches (Hz)

Mode no.	No mass patches		1 cm mass patches		2 cm mass patches		3 cm mass patches	
	Test	Theory[a]	Test	Theory[a]	Test	Theory[a]	Test	Theory[a]
1	2.45	2.499	2.26	2.338	2.13	2.211	2.03	2.108
2	13.53	14.106	12.72	13.413	12.31	13.016	12.15	12.783
3	34.60	35.510	32.3	34.099	31.76	33.492	31.59	33.239
4	64.41	66.306	61.69	63.793	61.12	63.009	61.02	62.814
5	108.48	110.618	104.53	106.716	103.68	105.888	103.6	105.808

[a] Present equivalent model.

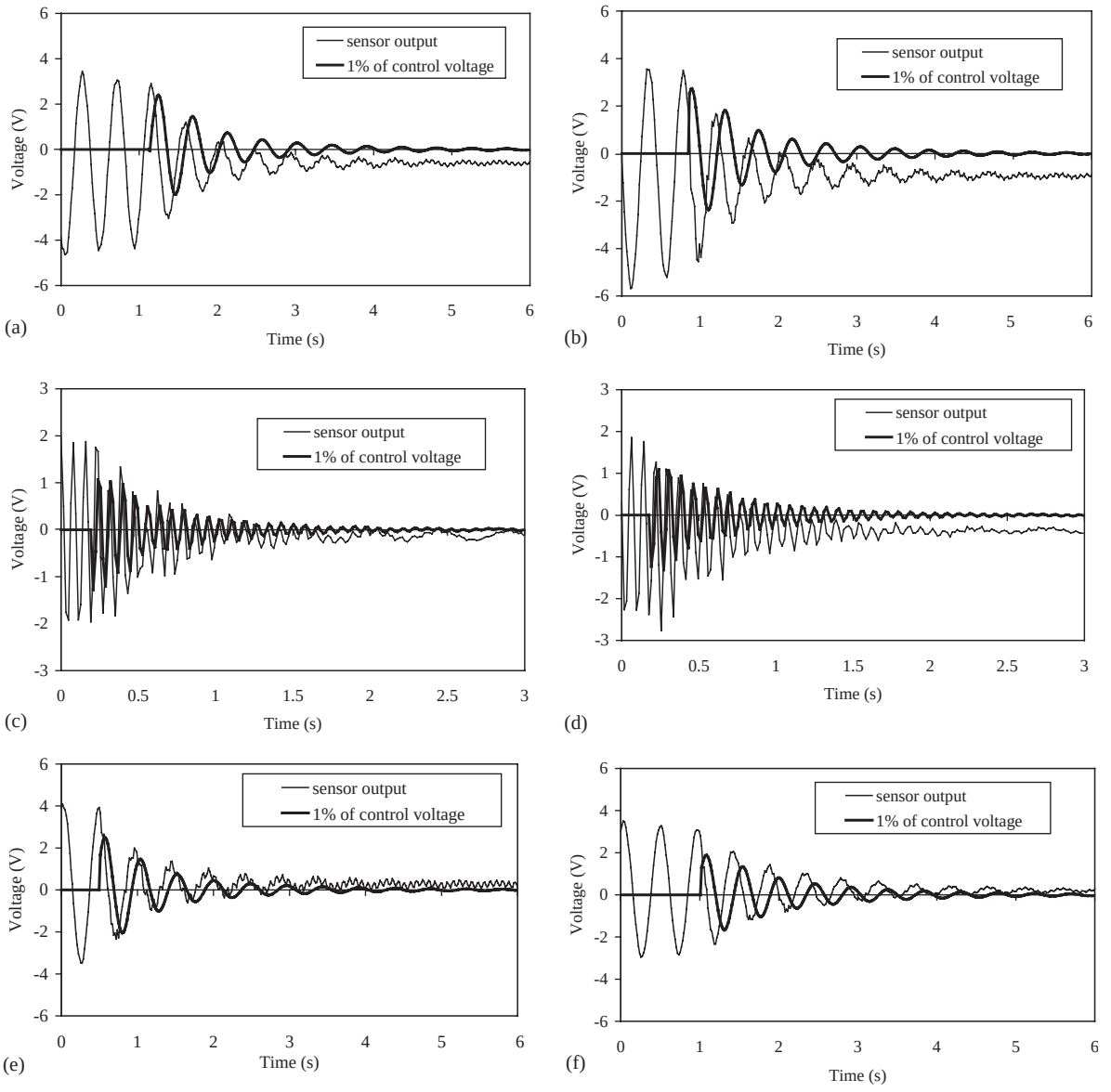

Fig. 11. Sensor output and control voltage in the experiment of vibration control of beam with different mass patches: (a) 1 cm mass patches, mode 1, controller using original frequency; (b) 1 cm mass patches, mode 1, controller using updated frequency; (c) 1 cm mass patches, mode 2, controller using original frequency; (d) 1 cm mass patches, mode 2, controller using updated frequency; (e) 2 cm mass patches, mode 1, controller using original frequency; (f) 2 cm mass patches, mode 1, controller using updated frequency; (g) 2 cm mass patches, mode 2, controller using original frequency; (h) 2 cm mass patches, mode 2, controller using updated frequency; (i) 3 cm mass patches, mode 1, controller using original frequency; (j) 3 cm mass patches, mode 1, controller using updated frequency; (k) 3 cm mass patches, mode 2, controller using original frequency; and (l) 3 cm mass patches, mode 2, controller using updated frequency.

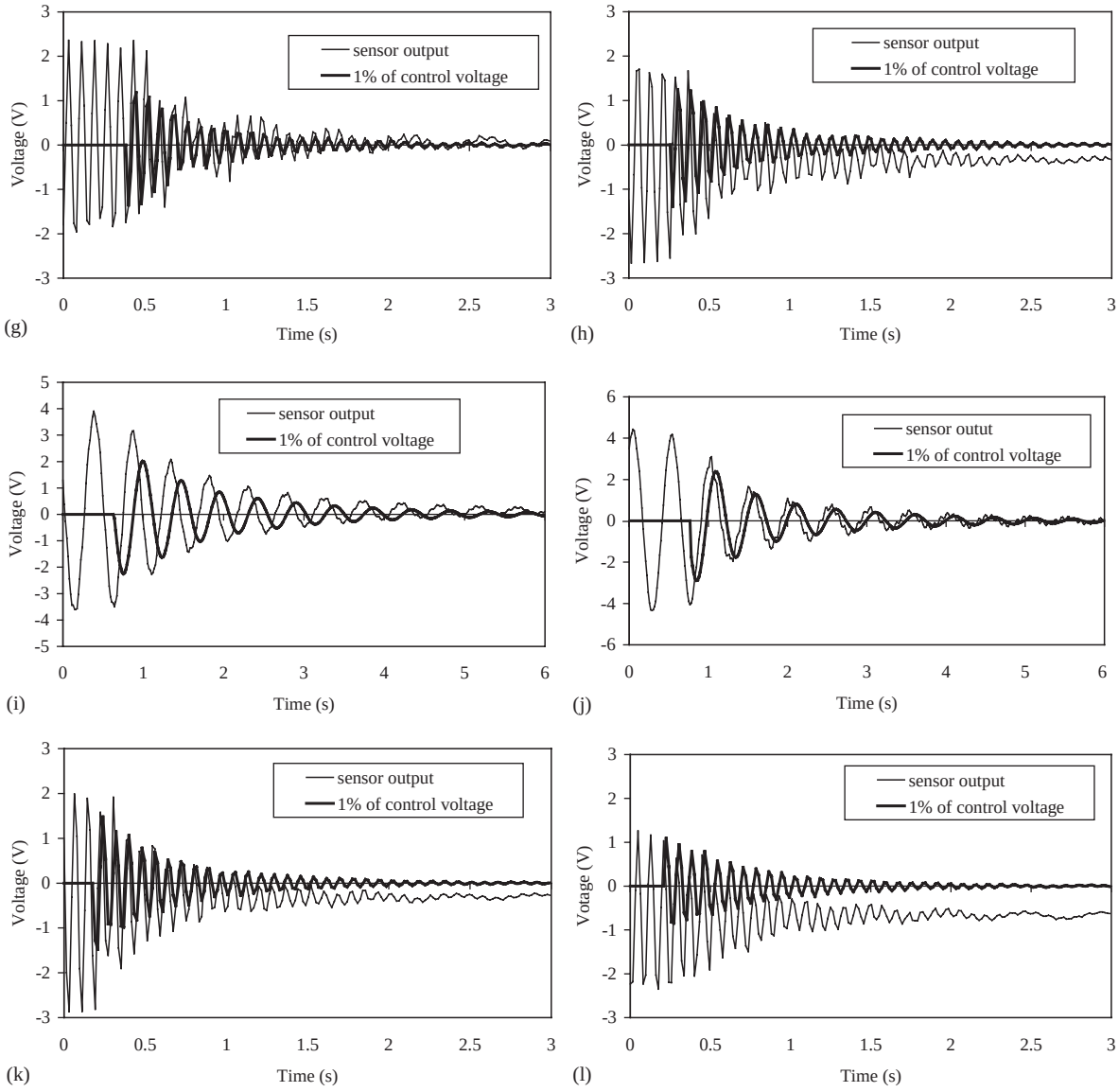

Fig. 11 (*continued*).

As shown in Fig. 12, when the modal frequencies are changed by attaching a pair of mass patches, the control efficiency of the original frequency-based controller will be reduced. For example, according to the experimental results, the first and the second modal damping ratios decrease 10% and 11% respectively due to the frequency change caused by a pair of 3 cm mass patch attachment at the free end of the test specimen. The reductions of the theoretical damping ratios due to the frequency shift are even larger. Fortunately, the deteriorative active control due to the frequency change can be compensated by detecting the frequencies and adaptively replacing the original ones in the controller with them. For instance, when constantly updating the

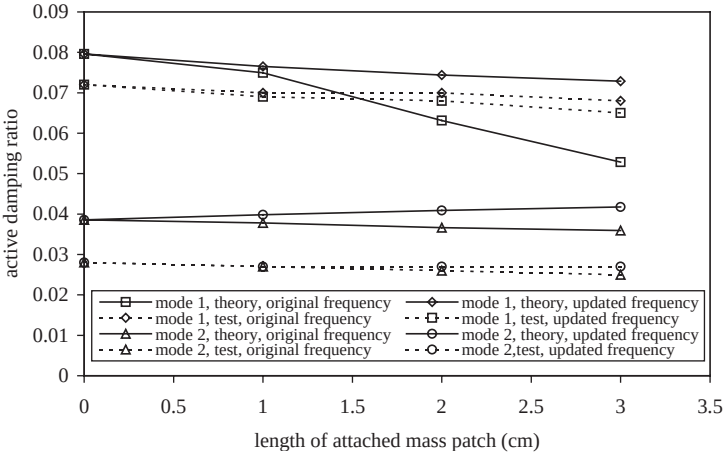

Fig. 12. Improvement of the active damping ratios caused by updating the frequencies in the controller.

frequencies in the controller as the mass attachment changes, the measured damping ratios for the first two controlled modes of the beam with a pair of 3 cm long mass patches increase 4.7% and 8% respectively. Theoretically, these increments of the active damping ratios are even larger and up to 37.9% and 16.3% for the controlled two modes respectively. Moreover, adaptively updating the frequencies in MVO controller can also improve the robustness of the active control. For example, when the first mode of the beam with a pair of 3 cm mass patches is controlled by the controller designed for the beam with no mass attachment, the second mode will be excited by a negative damping ratio -0.000386. After redesigning the controller according to the new frequency parameter, this negative damping ratio reduces to -0.00024, whose absolute value is much smaller than the natural damping ratio 0.0013, and hence the stability of the second mode is improved.

In practice, to prevent the control failure caused by the sudden debonding of the piezoelectric actuator or sensor patches, the frequency detection should be constantly detected and updated in the controller in every control loop. The computation process of the frequency detection, however, should be fast enough so that all the computation required by frequency detection and the control voltage design can be completed within the properly selected sampling interval. Except upgrading the hardware, some real-time algorithms [14] can be employed instead of the power spectrum method to estimate the frequencies quickly.

5. Conclusion

An equivalent model of the beams with partially debonded piezoelectric actuator and sensor patches and the solution scheme are given based on classical laminate theory and Timoshenko's beam theory. The continuity conditions at the interfaces between different composite beam segments as well as the interfaces between the perfectly bonded and debonded region are formulated for the purpose of displacement continuity and force balance. The effect of the edge debonding of an actuator patch on the modal shapes of the composite beam is studied. In

addition, a scheme to best restore the closed loop control, which has been worsened by the actuator debonding, is theoretically and experimentally demonstrated. Illustration examples show that the results obtained from the equivalent model are in good agreement with those from the full model and the experiment. The equivalent model can be employed incorporated with the full model if necessary.

Acknowledgements

The authors are grateful to the support of the Australia Research Council through a Large Grant (Grant No. A10009074).

References

[1] H. Luo, S. Hanagud, Dynamics of delaminated beams, *International Journal of Solids and Structures* 37 (2000) 1501–1519.
[2] Y. Zou, L. Tong, G.P. Steven, Vibration-based model-dependent damage (delamination) identification and health monitoring for composite structures—A review, *Journal of Sound and Vibration* 230 (2) (2000) 357–378.
[3] H. Fukunaga, N. Hu, F.K. Chang, Structural damage identification using piezoelectric sensors, *International Journal of Solids and Structures* 39 (2) (2002) 393–418.
[4] A. Chattopadhyay, H. Gu, D. Dragomir-Daescu, Dynamics of delaminated composite plates with piezoelectric actuators, *AIAA Journal* 37 (2) (1999) 248–254.
[5] C.E. Seeley, A. Chattopadhyay, Modeling of adaptive composites including debonding, *International Journal of Solids and Structures* 36 (1999) 1823–1843.
[6] S.H. Youn, J.H. Han, I. Lee, Neuro-adaptive vibration control of composite beams subject to sudden delamination, *Journal of Sound and Vibration* 238 (2) (2000) 215–231.
[7] A. Tylikowski, Effects of piezoactuator delamination on the transfer functions of vibration control systems, *International Journal of Solids and Structures* 38 (2001) 2189–2202.
[8] D. Sun, L. Tong, S.N. Atluri, Effects of piezoelectric sensor/actuator debonding on vibration control of smart beams, *International Journal of Solids and Structures* 38 (50–51) (2001) 9033–9051.
[9] D. Sun, L. Tong, Control stability analysis of smart beams with debonded piezoelectric actuator layer, *AIAA Journal* 40 (9) (2002) 1852–1859.
[10] M.S. Qatu, Theories and analyses of thin and moderately thick laminated composite curved beams, *International Journal of Solids and Structures* 30 (2) (1993) 2743–2756.
[11] C.-K. Lee, Theory of laminated piezoelectric plates for the design of distributed sensors/actuators. Part I: governing equations and reciprocal relationships, *Journal of Acoustical Society of America* 87 (3) (1990) 1144–1158.
[12] D. Sun, L. Tong, Closed-loop based detection of debonding of piezoelectric actuator/sensor patches in controlled smart beams, *International Journal of Solids and Structures* 40 (10) (2003) 2449–2471.
[13] L. Meirovitch, *Dynamics and Control of Structures*, Wiley-Interscience, New York, 1990 (Chapter 3).
[14] K.-H. Rew, S. Kim, I. Lee, Y. Park, Real-time estimations of multi-modal frequencies for smart structures, *Smart Materials and Structures* 11 (2002) 36–47.